Simulation of the color ratio associated with the backscattering of radiation by ice particles at the wavelengths of 0.532 and 1.064 μm

Lei Bi,[1] Ping Yang,[2] George W. Kattawar,[1] Bryan A. Baum,[3] Yong X. Hu,[4] David M. Winker,[4] R. Scott Brock,[5] and Jun Q. Lu[5]

Received 15 January 2009; revised 15 August 2009; accepted 1 September 2009; published 24 November 2009.

[1] This study explores a simulation of ice cloud optical properties similar to those observed using the Cloud-Aerosol Lidar with Orthogonal Polarization (CALIOP), a dual-wavelength (0.532 and 1.064 μm) lidar. The goal is to better understand the sensitivity of the color ratio (the ratio of the backscatter coefficients at the wavelengths of 1.064 and 0.532 μm) to ice particle habit. The single-scattering properties of randomly oriented hexagonal ice particles are simulated from the finite difference time domain (FDTD) method for particles with size parameters less than 50, and from an improved geometric optics method (IGOM) for particles with larger size parameters (a quantity proportional to the ratio of the particle characteristic dimension to the incident wavelength). Based on the assumption that ice particles are hexagonal particles, the color ratio values are found to be less than unity with a peak value near 0.7 for columns and 0.8 for plates. If spherical ice particles are assumed, the color ratio values can be larger than unity and may even approach 2 for many size distributions. The deviation in the value of the color ratio from unity is due to different distributions of size parameters for the two wavelengths, and to smaller single-scattering albedo values for large particles at 1.064 μm than at 0.532 μm. The present simulations of the color ratio for hexagonal columns are qualitatively consistent with measurements from a ground-based lidar, located at Hampton University in Hampton, Virginia, which peak near 0.88, but the two results differ quantitatively by 10–20 percent.

Citation: Bi, L., P. Yang, G. W. Kattawar, B. A. Baum, Y. X. Hu, D. M. Winker, R. S. Brock, and J. Q. Lu (2009), Simulation of the color ratio associated with the backscattering of radiation by ice particles at the wavelengths of 0.532 and 1.064 μm, *J. Geophys. Res.*, *114*, D00H08, doi:10.1029/2009JD011759.

1. Introduction

[2] The CALIPSO (Cloud-Aerosol Lidar and Infrared Pathfinder Satellite Observation) space-based platform includes three coaligned nadir-viewing instruments. One is the Cloud-Aerosol Lidar with Orthogonal Polarization (CALIOP), a dual-wavelength (0.532 and 1.064 μm) lidar. The primary goal of CALIPSO is to improve the understanding of the role of clouds and aerosols in weather, climate and air quality processes by providing global altitude-resolved optical properties [*Winker et al.*, 2003]. For CALIOP lidar algorithms [*Reagan et al.*, 2002; *Liu et al.*, 2004], the backscatter color ratio χ, a ratio of total backscatter coefficients at 1.064 μm and 0.532 μm channels under ice cloud conditions, is defined as follows:

$$\chi = \frac{\beta_{1.064}}{\beta_{0.532}} = \frac{\int_{D_{\min}}^{D_{\max}} \sigma_{sca,1.064}(D) P_{11,1.064}(\theta_s = 180^\circ, D) n(D) dD}{\int_{D_{\min}}^{D_{\max}} \sigma_{sca,0.532}(D) P_{11,0.532}(\theta_s = 180^\circ, D) n(D) dD}, \quad (1)$$

where D is the characteristic length of an ice particle that is usually specified in terms of its maximum dimension [*Yang et al.*, 2005]. In equation (1), $n(D)$ is the particle number density, σ_{sca} is the scattering cross section and P_{11} is the normalized phase function. The color ratio describes the spectral variations in the optical properties of a scattering medium of interest; the optical properties are based on the microphysical properties of the medium. In the scene classification algorithm [*Liu et al.*, 2004], the backscatter color ratio is one of the quantities required in the discrimination of aerosols from cloud particles and in the inference of the cloud thermodynamic phase.

[3] In the lidar calibration algorithm [*Reagan et al.*, 2002], the 0.532 μm channel is calibrated using the molecular backscattering signal. This method is not applicable to

[1]Department of Physics and Institute for Quantum Studies, Texas A&M University, College Station, Texas, USA.
[2]Department of Atmospheric Sciences, Texas A&M University, College Station, Texas, USA.
[3]Space Science and Engineering Center, University of Wisconsin-Madison, Madison, Wisconsin, USA.
[4]NASA Langley Research Center, Hampton, Virginia, USA.
[5]Department of Physics, East Carolina University, Greenville, North Carolina, USA.

0148-0227/09/2009JD011759$09.00

the 1.064 μm channel due to quite weak molecular backscattering at this wavelength. In practice, however, when cirrus clouds are selected as calibration targets, the 0.532 μm calibration coefficient can be transferred to the 1.064 μm channel. A prerequisite for this calibration technique is a priori knowledge of the color ratio values associated with ice clouds. Traditionally, it has been assumed that ice cloud optical properties in the visible through near-infrared region are spectrally independent, i.e., $\chi = 1$. Since the color ratio of ice clouds is a critical quantity in the CALIOP calibration algorithm, recent efforts [*Vaughan et al.*, 2008; *Tao et al.*, 2008] have been made to determine more realistic χ values. Ground-based lidar measurements of χ at Hampton University in Hampton, Virginia, were recorded from June 2006 through July 2007 [*Tao et al.*, 2008], and provided color ratio values of $\chi = 0.88 \pm 0.12$.

[4] We will focus on direct numerical calculations of χ, and will discuss the physical mechanisms having an influence on χ. We will also provide estimates of χ based on assumed ice particle geometries, including both hexagonal and spherical shapes. The present numerical simulations involve two stages: (1) calculation of ice particle single-scattering properties; and, (2) derivation of ice cloud bulk-scattering properties. The bulk-scattering properties are obtained by integrating individual ice particle scattering properties over a particle size distribution.

[5] The single- and bulk-scattering properties of ice clouds are calculated for various aspect ratios and size parameters at 0.532 and 1.064 μm wavelengths. One basic feature of hexagonal ice particles is that they have locally planar surfaces that lead to the enhancement of backscattering. In this study, we are concerned with the ratio of the spectral sensitivity in the direct backscattering direction. The particle sizes in ice clouds range from several to thousands of micrometers (μm). Therefore, for the single-scattering calculations, ice particles are assumed to have maximum dimensions that range from 2 to 10000 μm (the maximum dimension for a column, a plate or a sphere is its length, width or diameter, respectively). The value of the size parameter (a quantity proportional to the ratio of the particle maximum dimension to the incident wavelength) for the two wavelengths is quite different. The refractive indices for ice at the two wavelengths are $m_{0.532} = 1.3116 + 1.48243 \times 10^{-9}$, and $m_{1.064} = 1.3004 + 1.89839 \times 10^{-6}$ [*Warren and Brandt*, 2008]. Note that the imaginary part of the refractive index at 1.064 μm is larger than that at 0.532 μm by three orders of magnitude, which means that the absorption for large particles is stronger at 1.064 μm than at 0.532 μm. The single-scattering property computations for the nonspherical ice particles are based on a combination of the finite difference time domain (FDTD) method [*Yee*, 1966; *Yang and Liou*, 1996a; *Brock et al.*, 2005] and an improved geometric optics method (IGOM) [*Yang and Liou*, 1996b; *Yang et al.*, 2005]. For comparison, the single-scattering properties of ice spheres are calculated from the Lorenz-Mie theory.

[6] In previous calculations of the bulk-scattering properties [*Baum et al.*, 2005b], the single-scattering properties were calculated for 45 discrete sizes (called size bins). The single-scattering property database included a variety of ice habits including hexagonal plates, solid and hollow columns, 3D bullet rosettes, droxtals, and aggregates. In the intervening years since the formation of the database, a number of improvements have become available for light scattering calculations. For example, following *Mishchenko and Macke* [1998], a new treatment of polarized ray spreading has been incorporated for forward scattering that now makes obsolete the delta transmission term for rays that pass through two opposing (flat) facets of a hexagonal ice particle. The IGOM has been improved, especially for the efficiency factors [*Yang et al.*, 2007; *Bi et al.*, 2009] and the phase function at backscattering angles. The present simulations based on the new IGOM code are limited to hexagonal plates and columns. The discretization of the particle size has been enhanced with the new simulations.

[7] Given the individual particle single-scattering properties, the next step is to calculate bulk-scattering properties that are more representative of ice clouds, from which the color ratio values are derived. The bulk-scattering properties, and in particular the backscattering cross section per unit volume, are calculated by integrating individual particle scattering properties over a given set of particle size and habit distributions. For this study, ice habits are assumed to be hexagonal columns, plates or spheres, and a mixture of habits is not considered because a full set of scattering properties is unavailable for a more extensive set of habits. Future work will explore similar color ratio calculations for mixtures of habits.

[8] Integration of ice particle single-scattering properties is based on a set of 1117 particle size distributions (PSDs) from the various field campaigns described by *Baum et al.* [2005a]. These campaigns include the First International Satellite Cloud Climatology Project Regional Experiment (FIRE-I), held in 1986 and (FIRE-II), held in 1991; the Atmospheric Radiation Measurement (ARM) Intensive Operation Period (IOP), held in 2000 near Lamont, Oklahoma; the Tropical Rainfall Measuring Mission (TRMM) validation campaign in the Kwajalein Islands, the Kwajalein Experiment (KWAJEX), held in 1999; and the Cirrus Regional Study of Tropical Anvils and Cirrus Layers (CRYSTAL) Florida Area Cirrus Experiment (FACE), held in 2002. The data from the FIRE and ARM IOP campaigns were obtained from midlatitude, primarily synoptic, cirrus, while the other data were obtained from tropical anvil (TRMM) or tropical tropopause cirrus (CRYSTAL-FACE). The ice water contents for this set of PSDs range from approximately 10^{-3} to 1 g m^{-3}, and the median mass diameters range from 50 to 2000 μm.

[9] The paper is organized as follows. Section 2 describes the numerical methods for the single-scattering calculations. Particular attention is given to the improvements of the geometric optics algorithm, which leads to a more accurate approach to computing the scattering properties of nonspherical particles over a complete range of size parameters from the Rayleigh to the geometric optics regimes. In Section 3, we present the single-scattering properties computed with the "unified theory" whose concept was first developed by *Liou et al.* [1999], the bulk-scattering properties, and the color ratios of ice clouds simulated with hexagonal particles of different aspect ratios. Physical mechanisms that influence the values of χ are also ana-

lyzed. Section 4 discusses the conclusions reached from the present study on color ratios of ice clouds.

2. Numerical Methods for Single Scattering

[10] For an ice sphere of diameter D, the backscattering cross section can be formulated analytically based on the Lorenz-Mie theory [*Bohren and Huffman*, 1983] as follows:

$$\sigma_b(m, \lambda, \mathrm{D}) = 4\pi |S_1(m, \mathrm{x} = kD/2,\ \theta_s = 180^\circ)|^2 / k^2, \quad (2)$$

where λ is the wavelength, k is the wave number and equal to $2\pi/\lambda$, and S_1 is the element of the amplitude scattering matrix as a function of complex refractive index m, the size parameter x and the scattering angle θ_s. Note that $S_2 = -S_1$ at $\theta_s = 180^\circ$. Therefore, the backscatter color ratio defined in equation (1) is given by

$$\chi = \frac{\int_{D_{\min}}^{D_{\max}} \sigma_b(m_{1.064}, 1.064, D) n(\mathrm{D}) d\mathrm{D}}{\int_{D_{\min}}^{D_{\max}} \sigma_b(m_{0.532}, 0.532, D) n(\mathrm{D}) d\mathrm{D}}. \quad (3)$$

[11] The Lorenz-Mie code written by *Bohren and Huffman* [1983] is employed to calculate S_1.

[12] Unlike spheres, for which the single-scattering properties can be calculated analytically from the Lorenz-Mie theory, there is no single method that can provide the single-scattering properties of hexagonal particles over a large range of size parameters [*Mishchenko and Hovenier*, 1999]. A combination of the FDTD and IGOM methods is applied to the present calculations [*Liou et al.*, 1999; *Yang et al.*, 2005]. This "unified approach" to the scattering simulations was first introduced by *Liou et al.* [1999]. Note that other exact numerical methods, such as the T matrix method [*Mishchenko and Travis*, 1994; *Havemann and Baran*, 2001], the pseudospectral time domain method (PSTD) [*Chen et al.*, 2008] and the discrete dipole approximate method (DDA) [*Purcell and Pennypacker*, 1973], may also be used to derive the single-scattering properties of small hexagonal particles.

[13] Recently, some important improvements associated with the FDTD and IGOM methods have been achieved. Previously, the FDTD method could be employed for particles having size parameters up to about 20, beyond which point a tremendous demand on computational resources essentially prohibited the numerical simulations. A parallelized version of the FDTD method [*Brock et al.*, 2005] is now available, permitting the use of supercomputers to perform the simulations for larger particles with size parameters up to 50. Additionally, the IGOM method has been systematically improved in several ways. First, earlier calculations using the IGOM led to discontinuities in the efficiency factors and the presence of a delta transmission term at visible shortwave infrared (SWIR) wavelengths. The discontinuity in the efficiency factor was due in part to the previous treatment of the particle above-edge effect [*Mitchell et al.*, 2001]. These artifacts have been mitigated in the current version, thus extending the use of the IGOM to particles having smaller size parameters [*Yang et al.*, 2007; *Bi et al.*, 2009]. Additionally, the IGOM now produces more accurate asymptotic values for very large particles. Consideration of the edge effect results in a smooth transition of the efficiency factors computed from the IGOM to those of the FDTD method. The delta transmission term is no longer present in the present IGOM results due to a new treatment of forward scattering that more properly accounts for the ray-spreading effect in the computation of the far field. In the following section, we specifically discuss the improvement associated with the treatment of the ray-spreading effect [*Muinonen*, 1989; *Yang and Liou*, 1996b] that is essential to the backscattering calculations in the present study.

[14] *Yang and Liou* [1996b] presented a simplified algorithm of mapping the near field to the far field to account for the ray spreading effect for randomly oriented particles. In this algorithm, the degree of ray spreading is associated with the cross-sectional area of the rays. The effect of ray spreading decreases as the cross section of a ray increases. Therefore, the phase matrix computed from the IGOM method should transition to that computed from the conventional geometric optics method [*Cai and Liou*, 1982; *Takano and Liou*, 1989; *Macke*, 1993]. Here, the cross-sectional area of a ray is an important parameter. As articulated by *van de Hulst* [1957], the ray cross-sectional area is physically related to the dimension of the scattering particle. For a ray with a length l (or, the propagation distance of a localized wave), the base area should be on the order of $l\lambda$ if $l \gg \lambda$, where λ is the wavelength of the incident light. Therefore, the ray concept is still more or less reasonable within particles with a size parameter of $\sim$20. Note this is the region where rigorous numerical methods (e.g., FDTD and DDA) are still computationally practical. The IGOM method, which has been improved to account for the ray spreading effect more accurately, is an essential part of the "unified approach" [*Liou et al.*, 1999] for computing the single-scattering properties of randomly oriented particles over a complete range of size parameters.

[15] When a localized wave emerges from the particle, it propagates a long distance to reach the far-field zone ($l\lambda \rightarrow \infty$). In this case, the ray concept is no longer valid because of the finite cross section of the ray that may spread around its outgoing direction according to the Huygens principle in physical optics. By considering the ray-spreading effect, the equation that relates the phase matrix from the conventional geometric optics approach and the improved geometric optics method can be formulated as:

$$P(\theta, \phi) = \iint C(\theta_t, \phi_0) \Xi(\theta, \theta_t, \phi, \phi_0) \tilde{P}(\theta_t, \phi_0) L(\phi_t = \phi - \phi_0) \cdot \sin\theta_t d\theta_t d\phi_0, \quad (4)$$

where $\tilde{P}(\theta_t, \phi_0)$ is the phase matrix from the conventional geometric optics method, θ_t is the scattering angle and ϕ_0 is the azimuthal angle; $P(\theta, \phi)$ is the phase matrix for the IGOM but with a different scattering angle θ and azimuthal angle ϕ; and, L is a matrix associated with the rotation of scattering plane that is given by

$$L = \begin{bmatrix} 1 & 0 & 0 & 0 \\ 0 & \cos(2\phi_t) & \sin(2\phi_t) & 0 \\ 0 & -\sin(2\phi_t) & \cos(2\phi_t) & 0 \\ 0 & 0 & 0 & 1 \end{bmatrix}, \quad (5)$$

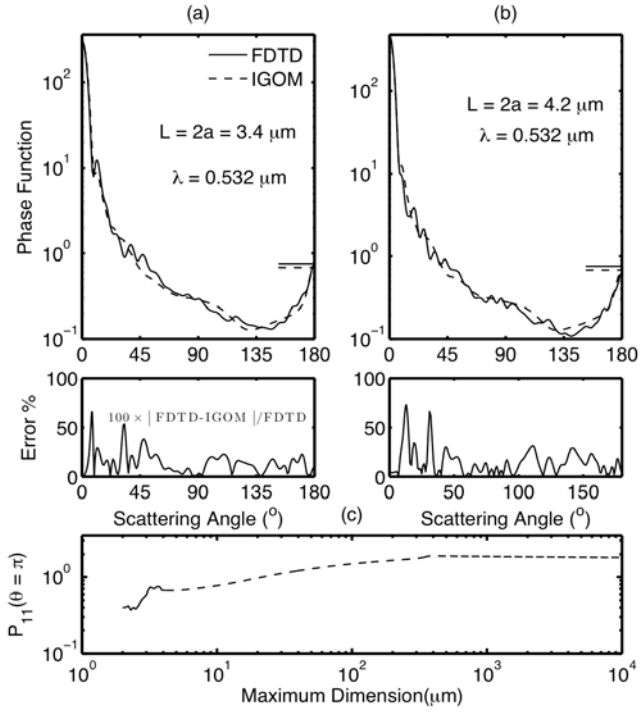

Figure 1. Comparison of the phase function computed from the FDTD and IGOM for compact hexagonal columns at the wavelength of 0.532 μm and size of (a) 3.4 μm and (b) 4.2 μm. (c) Values of the phase function at the backscattering direction as a function of maximum dimension of particles from 2 to 10,000 μm. L and a are the length and semiwidth, respectively, of the hexagonal particles.

where ϕ_t is considered positive with a range from 0 to 2π. Ξ is another matrix associated with the ray-spreading effect and is given by

$$\Xi = \begin{bmatrix} \Xi_{11} & \Xi_{12} & \Xi_{13} & 0 \\ \Xi_{21} & \Xi_{22} & \Xi_{23} & 0 \\ \Xi_{31} & \Xi_{32} & \Xi_{33} & 0 \\ 0 & 0 & 0 & \Xi_{44} \end{bmatrix}. \tag{6}$$

[16] The coefficient $C(\theta_t, \phi_0)$ is introduced to guarantee the conservation of energy for the mapping algorithm. For the color ratio study, we are concerned with P_{11} for randomly oriented hexagonal columns. The matrix equation (4) is simplified to a scalar equation as follows:

$$P_{11}(\theta) = \int\int C(\theta_t)\left[\Xi_{11}(\theta, \theta_t, \phi_t)\tilde{P}_{11}(\theta_t) + \Xi_{12}(\theta, \theta_t, \phi_t)\tilde{P}_{21}(\theta_t)\right] \cdot \sin\theta_t d\theta_t d\phi_t. \tag{7}$$

[17] Elements of Ξ are presented in the Appendix. Equations (4)–(7) represent a generalization of equation (51) of *Yang and Liou* [1996b]. For the numerical implementation, there are two concerns related to the stability and accuracy of the simplified mapping algorithm. The first concern is associated with the introduced coefficient. For each θ_t, we should normalize the contribution to the scattering angle θ. In previous studies, C is assumed to be independent of θ_t and is removed from the integral. We find that $C(\theta_t)$ is essential to the accuracy of the backscattering due to its much smaller value than its counterpart for the forward scattering. The second concern is about the number (N) of points selected over θ_t to perform the numerical integration. For large particles, the cross section of the ray is so large that the kernel Ξ has a sharp peak in the direction of (θ_t, 0). If N is not sufficiently large in this region, a convergent numerical solution may not be obtained.

3. Results and Discussion

[18] Figure 1 demonstrates the applicability of the "unified theory" [*Liou et al.*, 1999] for the calculation of scattering properties of ice particles from small to very large sizes. The phase functions computed from the FDTD and IGOM methods are compared in Figures 1a and 1b for two different sizes of compact hexagonal ice particles ($L/2a = 1$) at a wavelength of 0.532 μm. The results indicate that the IGOM method can provide a close approximation of the phase function, except that some oscillations cannot be produced where large relative errors are observed. In this study, we are concerned with values of the phase function at the direct backscattering angle observed by a ground-based lidar. Figure 1c shows $P_{11}(\theta = \pi)$ as a function of particle maximum dimension. The FDTD method was used for small particles with maximum dimensions smaller than 4.2 μm (size parameter $\sim$50), and the IGOM method was used for large particles with size parameters larger than 50. The backscattering phase function of ice particles can be simulated reliably with the "unified approach." Note that P_{11} presented here is the normalized phase function. For very large particles, the ray spreading effect can be neglected. The phase function obtained from the IGOM transitions to that obtained from the conventional geometric optics method; therefore, the value of the normalized phase function in the backscattering direction tends to be a constant asymptotically.

[19] Shown in Figure 2 are the scattering efficiency factors and ratios of backscattering cross sections at the wavelengths of 1.064 μm and 0.532 μm as functions of particle size for hexagonal particles for three typical aspect ratios. As demonstrated in Figures 2a, 2c, and 2e, the values of the scattering efficiency factors are quite different at the two wavelengths. For small particles, a displacement of peaks is apparent. This is due to different distributions of the size parameters at the two wavelengths. The scattering efficiency factors for small and moderate particles are also quite sensitive to aspect ratios. For very large particles with maximum dimensions larger than 2000 μm, the scattering efficiency factors are smaller at 1.064 μm than at 0.532 μm. As noted earlier, this behavior is due to the increased absorption by ice particles at the 1.064 μm channel. The lower three panels show the ratios of backscattering cross sections at the two wavelengths for a range of particle sizes. The common feature of Figures 2a, 2c, and 2e is that values of the color ratio are generally smaller than 1 for small to moderate particles. This behavior is due to a larger degree of ray spreading at the 1.064 μm channel. The ratio decreases significantly when the maximum particle dimension is larger than 2000 μm. This feature is consistent with the behavior of the scattering efficiency because absorption is

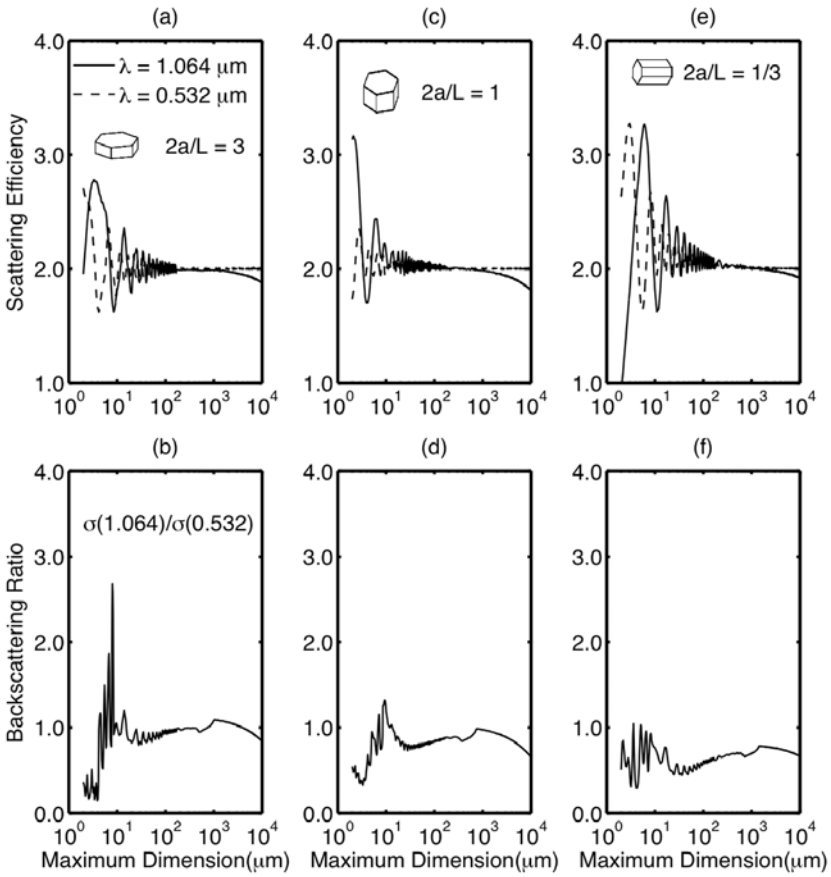

Figure 2. (a) Scattering efficiency factor and (b) backscattering ratio as functions of maximum dimension of the hexagonal particles with an aspect ratio of 3. Hexagonal particles having aspect ratios of (c and d) 1 and (e and f) 1/3.

pronounced at the 1.064 μm channel. Oscillations of the backscattering cross sections for small particles can reach a larger value, e.g., 2.7 in Figure 2b.

[20] For comparison with hexagonal ice particles, Figure 3 shows the scattering efficiency of ice spheres at the two wavelengths as well as backscattering cross sections and distributions of color ratio values. The overall oscillation pattern of the scattering efficiency factors and its asymptotic behavior are similar to those of hexagonal columns. The backscattering cross sections display strong oscillations with particle size. A distribution of color ratio values is obtained from the bulk-scattering calculations, i.e., integrating over particle size distributions. The color ratio values range from 0.4 to 1.9. Due to the highly oscillating nature of the backscattering cross sections, the size bin is assumed to be 0.005 μm for the integral.

[21] The aspect ratio of ice particles has been investigated in previous studies. For columns, the relation of width and length is defined by *Yang et al.* [2001] according to observations [*Ono*, 1969; *Auer and Veal*, 1970] given by:

$$2a = \begin{cases} \mathrm{L}, & \mathrm{L} \le 40\,\mu\mathrm{m}, \\ \mathrm{L}\exp[-0.017835(\mathrm{L}-40)], & 40 < \mathrm{L} \le 50\,\mu\mathrm{m}, \\ 5.916\mathrm{L}^{1/2}, & \mathrm{L} > 50\ \mu\mathrm{m}. \end{cases} \quad (8)$$

where a is the semiwidth and L is the length. For plates, we use the following relationship:

$$\mathrm{L} = \begin{cases} 2a, & \mathrm{a} \le 2\,\mu\mathrm{m}, \\ 0.4453a + 3.1093, & 2 < \mathrm{L} \le 5\,\mu\mathrm{m}, \\ 2.4883a^{0.474}, & \mathrm{a} > 5\ \mu\mathrm{m}. \end{cases} \quad (9)$$

[22] This relationship for the aspect ratio was employed by *Yang et al.* [2005] to develop a database of the scattering and absorption properties of the particles. The aspect ratio relationship for semiwidth larger than 5 μm is adapted from *Pruppacher and Klett* [1980].

[23] Figure 4 shows the results for columns. The scattering efficiency factors for large particles at the two wavelengths are basically the same but are different from the hexagonal particles with fixed aspect ratios studied previously. For the aspect ratios given in equations (8) and (9), the volume of particles with a large maximum dimension is smaller than that of fixed aspect ratios; therefore, the weak absorption at 1.064 μm is not pronounced. The factor that influences the value of the color ratio is restricted to different distributions of size parameters.

[24] Figure 5 shows the results for plates. The values of the color ratio for plates tend to be larger than those for columns. Color ratio values are smaller than unity with the

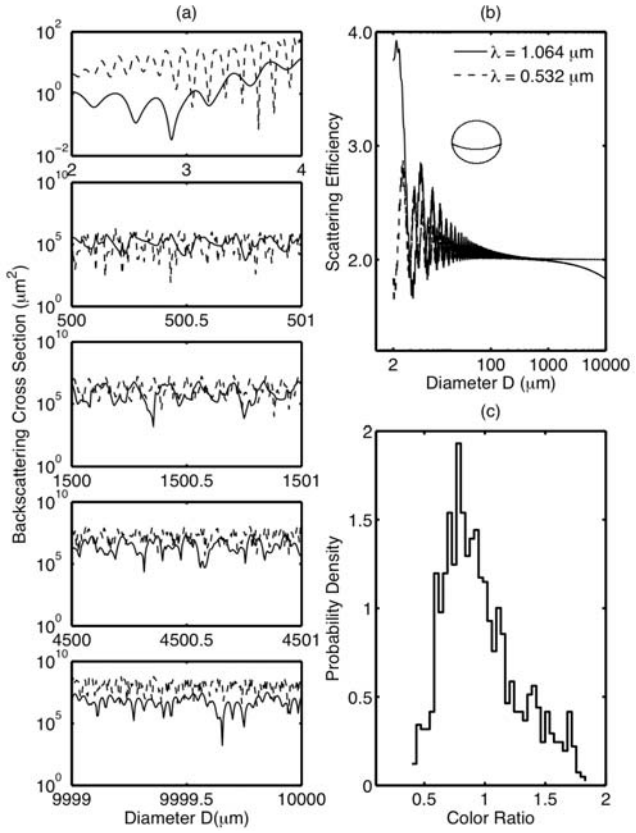

Figure 3. (a) Backscattering cross sections of spheres at 1.064 μm and 0.532 μm. (b) Scattering efficiency factors of spheres at the two wavelengths. (c) Distribution of color ratios calculated from 1117 individual particle size distributions obtained from various field campaigns.

peak value near 0.8. As expected, comparison of the results shown in Figures 3, 4 and 5 indicates that the color ratio values for spheres are quite different from those of hexagonal particles. For both plates and columns, the color ratios are found to be sensitive to particle aspect ratios. Values of color ratios larger than unity are seldom observed in our calculations. This behavior is consistent with ice cloud measurements from the ground-based lidar at Hampton University.

[25] The effective particle size, defined as the ratio of the third moment to the second moment, is usually employed to characterize a particular size distribution [*Foot*, 1988; *Francis et al.*, 1994]:

$$D_{eff} = \frac{3}{2}\frac{\int_{D_{\min}}^{D_{\max}} V(D)n(D)dD}{\int_{D_{\min}}^{D_{\max}} A(D)n(D)dD}, \qquad (10)$$

where V is the volume and A is the average projected area. Figure 6a shows the color ratio as a function of effective particle size. The values of the color ratio for spheres can be larger than 1 and may be as large as 2 for smaller effective diameters. The values are smaller than unity when the effective diameter is larger than 400 μm. For plates, the values increase with effective size and approach unity. As

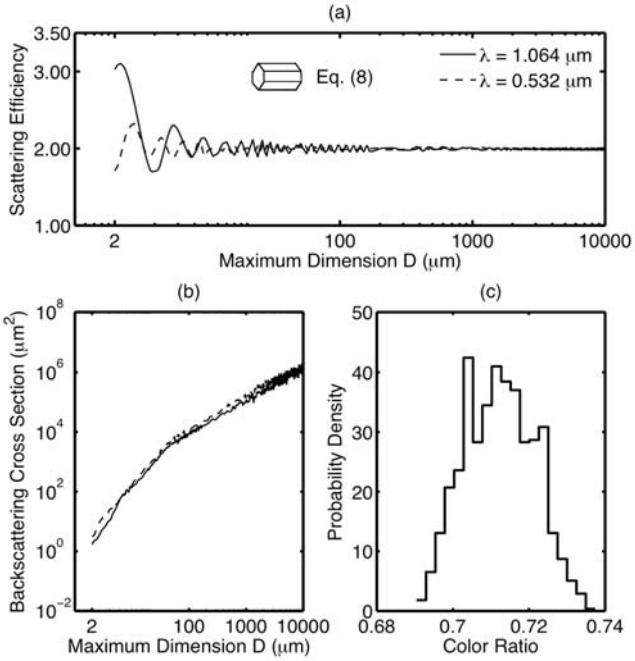

Figure 4. (a) Scattering efficiency factors of hexagonal columns with size-dependent aspect ratios defined in equation (8) at 1.064 μm and 0.532 μm. (b) Backscattering cross sections at the two wavelengths. (c) Distribution of color ratios calculated from the same size distributions as employed in Figure 3c.

noted previously, the color ratio values are smaller for columns than those for plates. Figure 6b shows simulated probability distributions of the color ratio in comparison with that based on ground-based lidar measurements [*Tao et al.*, 2008]. For both columns and plates, the entire range of color ratio values is consistent with ground-based lidar

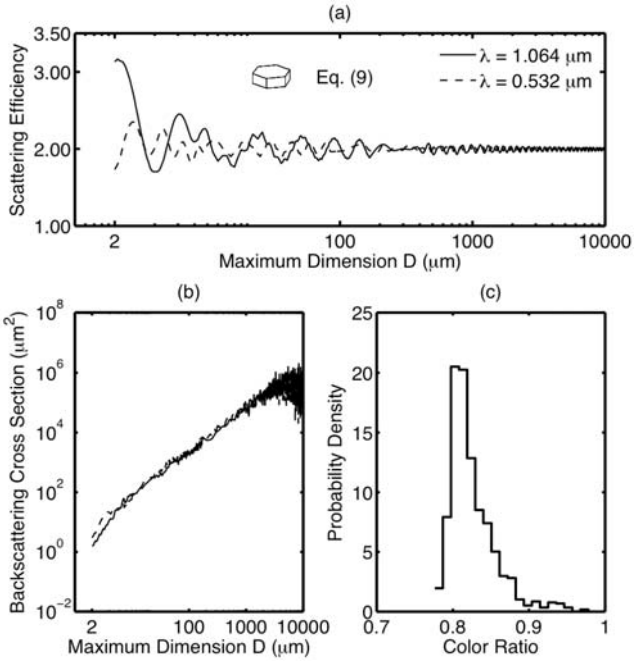

Figure 5. Same as Figure 4, except for hexagonal plates with size-dependent aspect ratios defined in equation (9).

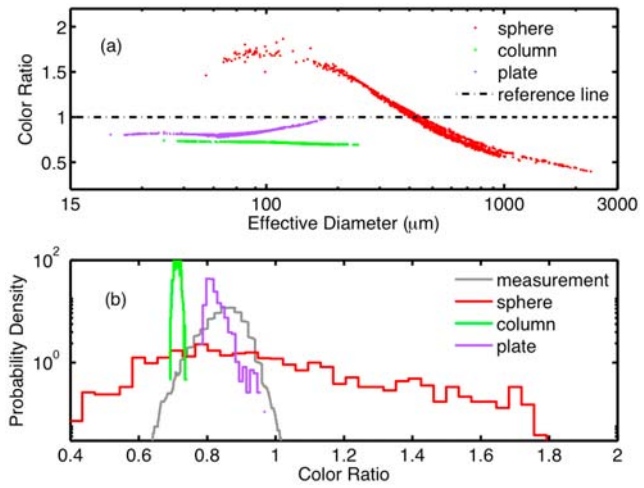

Figure 6. (a) Color ratio as a function of effective diameter for spheres, columns and plates. (b) Comparison of simulated probability distributions of color ratio with ground-based lidar measurements from Hampton University [*Tao et al.*, 2008].

measurements. As mentioned previously, the color ratio for ice spheres has a broad range of values ranging from 0.4 to ~2. Note that numerical investigations presented here are based on a simple simulation model that captures the main physics of ice particles. In fact, realistic ice particles tend to have more complex shapes and include hollow cavities as well as surface roughening. Furthermore, depending on the updraft velocity in the environment where the ice particles are located, the ice particles may not be randomly oriented in the atmosphere. These effects will be evaluated in future research.

4. Summary and Conclusions

[26] This study explores ice cloud backscattering simulations similar to those that may be observed using a dual-wavelength lidar (0.532 and 1.064 μm). The focus is on a quantity known as the color ratio, which is defined as the ratio of backscatter coefficients at wavelengths of 1.064 and 0.532 μm. This study is aimed at a better understanding of the sensitivity of the color ratio to ice particle habit by employing the single-scattering and bulk-scattering properties of hexagonal ice particles. The single-scattering properties of randomly oriented hexagonal particles with various aspect ratios and maximum dimensions from 2 to 10000 μm are simulated from the FDTD (finite difference time domain) method for small particles and the IGOM (improved geometric optics method) for large particles. The IGOM method has been systematically improved so that there are now no discontinuities in the efficiency factors when transitioning between FDTD and IGOM results. Furthermore, a new treatment of ray spreading replaces a less accurate treatment of mapping the near field to the far field. As a result, there is no longer a delta transmission term at visible shortwave infrared (SWIR) wavelengths. A total of 1117 particle size distributions from a number of field campaigns are employed to obtain a distribution of backscatter color ratio values. Based on the assumption that ice particles are hexagonal columns or plates, it is found that the color ratio values are less than 1 with a peak value near 0.7 for columns and 0.8 for plates. For comparison, the color ratio values are computed for ice spheres. When the effective diameter is smaller than ~400 μm, the color ratio is larger than unity and can even approach 2 for size distributions that are dominated by small particles. For larger effective diameters, the color ratio is smaller than unity and decreases with increasing effective diameter.

[27] The deviation of the color ratio from unity is due to different distributions of size parameters for the two wavelengths and smaller single-scattering albedo values for large particles at the 1.064 μm channel. The color ratio values found for hexagonal columns are qualitatively consistent with measurements from a ground-based lidar, housed at Hampton University in Hampton, Virginia, that peak near 0.88, but the two results differ quantitatively by 10–20 percent. Future research will continue the investigation of the color ratio by (1) extending the ice habits to include 3D bullet rosettes, aggregates of plates and other complex shapes, (2) exploring the effect of inclusions in the ice particles, and (3) exploring the effect of surface roughness on the ice particles.

Appendix A: Elements of Ray Spreading Matrix in Equation (4)

[28] A two-by-two matrix Ξ is defined by

$$\Xi = \begin{bmatrix} \Xi_2 & \Xi_3 \\ \Xi_4 & \Xi_1 \end{bmatrix}.$$

[29] The four elements of this matrix are given by,

$$\Xi_1 = h\cos\phi_t,$$
$$\Xi_2 = h\cos\theta\cos\theta_t\cos\phi_t + h\sin\theta\sin\theta_t,$$
$$\Xi_3 = -h\cos\theta\sin\phi_t,$$
$$\Xi_4 = h\cos\theta_t\sin\phi_t,$$

where h is the same as equation (46b) of *Yang and Liou* [1996b]. Note that the matrix Ξ is different from equation (A8) of *Yang and Liou* [1996b] by a factor h. The elements of ray-spreading matrix can be formulated as follows:

$$\Xi_{11} = \frac{1}{2}\left(\Xi_1^2 + \Xi_2^2 + \Xi_3^2 + \Xi_4^2\right),$$
$$\Xi_{12} = \frac{1}{2}\left(\Xi_2^2 - \Xi_1^2 + \Xi_4^2 - \Xi_3^2\right),$$
$$\Xi_{21} = \frac{1}{2}\left(\Xi_2^2 - \Xi_1^2 - \Xi_4^2 + \Xi_3^2\right),$$
$$\Xi_{22} = \frac{1}{2}\left(\Xi_2^2 + \Xi_1^2 - \Xi_4^2 - \Xi_3^2\right),$$
$$\Xi_{13} = \Xi_2\Xi_3 + \Xi_1\Xi_4,$$
$$\Xi_{23} = \Xi_2\Xi_3 - \Xi_1\Xi_4,$$
$$\Xi_{31} = \Xi_2\Xi_4 + \Xi_1\Xi_3.$$
$$\Xi_{32} = \Xi_2\Xi_4 - \Xi_1\Xi_3,$$
$$\Xi_{33} = \Xi_1\Xi_2 + \Xi_3\Xi_4,$$
$$\Xi_{44} = \Xi_1\Xi_2 - \Xi_3\Xi_4.$$

[30] For randomly oriented particles, Ξ_{11} and Ξ_{12} are reduced to equation (51) of *Yang and Liou* [1996b].

[31] **Acknowledgments.** This research is supported by a NASA grant (NNL06AA01A) and a subcontract from the University of Wisconsin (G074605). The effort on the single-scattering computation involved in this project is partly supported by a grant (ATM-0239605) from the National Science Foundation (NSF) Physical and Dynamic Meteorology Program managed by Bradley Smull. George W. Kattawar's research is also supported by the Office of Naval Research under contract N00014-06-1-0069. Support for Bryan Baum is provided through NASA grant NNX08AF81G. Jun Lu's research is supported by National Institutes of Health (NIH) grants (1R15GM70798-01 and 2R15GM70798-02). A portion of the numerical simulations involved in this study was carried out using NASA's supercomputing facility.

References

Auer, A. H., Jr., and D. L. Veal (1970), The dimension of ice crystals in natural clouds, *J. Atmos. Sci.*, *27*, 919–926, doi:10.1175/1520-0469(1970)027<0919:TDOICI>2.0.CO;2.

Baum, B. A., A. J. Heymsfield, P. Yang, and S. T. Bedka (2005a), Bulk scattering properties for the remote sensing of ice clouds. Part I: Microphysical data and models, *J. Appl. Meteorol.*, *44*, 1885–1895, doi:10.1175/JAM2308.1.

Baum, B. A., P. Yang, A. J. Heymsfield, S. Platnick, M. D. King, and S. T. Bedka (2005b), Bulk scattering models for the remote sensing of ice clouds. Part 2: Narrowband models, *J. Appl. Meteorol.*, *44*, 1896–1911, doi:10.1175/JAM2309.1.

Bi, L., P. Yang, G. W. Kattawar, and R. Kahn (2009), Single-scattering properties of triaxial ellipsoidal particles for a size parameter range from the Rayleigh to geometric-optics regimes, *Appl. Opt.*, *48*, 114–126, doi:10.1364/AO.48.000114.

Bohren, C. F., and D. R. Huffman (1983), *Absorption and Scattering of Light by Small Particles*, Wiley-Intersci., Hoboken, N. J.

Brock, R. S., X. Hu, P. Yang, and J. Q. Lu (2005), Evaluation of parallel FDTD code and application to modeling of light scattering by deformed red blood cells, *Opt. Express*, *13*, 5279–5292, doi:10.1364/OPEX.13.005279.

Cai, Q., and K. N. Liou (1982), Polarized light scattering by hexagonal ice crystals: Theory, *Appl. Opt.*, *21*, 3569–3580, doi:10.1364/AO.21.003569.

Chen, G., P. Yang, and G. W. Kattawar (2008), Application of the pseudospectral time-domain method to the scattering of light by nonspherical particles, *J. Opt. Soc. Am. A Opt. Image Sci. Vis.*, *25*, 785–790, doi:10.1364/JOSAA.25.000785.

Foot, J. S. (1988), Some observations of the optical properties of clouds: II. Cirrus, *Q. J. R. Meteorol. Soc.*, *114*, 145–164, doi:10.1002/qj.49711447908.

Francis, P. N., A. Jones, R. W. Saunders, K. P. Shine, A. Slingo, and Z. Sun (1994), An observational and theoretical study of the radiative properties of cirrus: Some results from ICE'89, *Q. J. R. Meteorol. Soc.*, *120*, 809–848, doi:10.1002/qj.49712051804.

Havemann, S., and A. J. Baran (2001), Extension of T-matrix to scattering of electromagnetic plane waves by non-axisymmetric dielectric particles: Application to hexagonal ice cylinders, *J. Quant. Spectrosc. Radiat. Transfer*, *70*, 139–158, doi:10.1016/S0022-4073(00)00127-8.

Liou, K. N., Y. Takano, and P. Yang (1999), Light scattering and radiative transfer in ice crystal clouds: Applications to climate research, in *Light Scattering by Nonspherical Particles: Theory, Measurements and Applications*, edited by M. I. Mishchenko, J. W. Hovenier, and L. D. Travis, pp. 417–449, Academic, San Diego, Calif.

Liu, Z., M. A. Vaughan, D. M. Winker, C. A. Hostetler, L. R. Poole, D. Hlavka, W. Hart, and M. McGill (2004), Use of probability distribution functions for discriminating between cloud and aerosol in lidar backscattering data, *J. Geophys. Res.*, *109*, D15202, doi:10.1029/2004JD004732.

Macke, A. (1993), Scattering of light by polyhedral ice crystals, *Appl. Opt.*, *32*, 2780–2788, doi:10.1364/AO.32.002780.

Mishchenko, M. I., and A. Macke (1998), Incorporation of physical optics effects and computation of the Legendre expansion for ray-tracing scattering functions involving δ-function transmission, *J. Geophys. Res.*, *103*, 1799–1805, doi:10.1029/97JD03121.

Mishchenko, M. I., and L. D. Travis (1994), Light scattering by polydispersions of randomly oriented spheroids with sizes comparable to wavelengths of observations, *Appl. Opt.*, *33*, 7206–7225, doi:10.1364/AO.33.007206.

Mishchenko, M. I., J. W. Hovenier, and L. D. Travis (Eds.) (1999), *Light Scattering by Nonspherical Particles: Theory, Measurements, and Applications*, Academic, San Diego, Calif.

Mitchell, D. L., W. P. Arnott, C. Schmitt, A. J. Baran, S. Havemann, and Q. Fu (2001), Contributions of photon tunneling to extinction in laboratory grown hexagonal columns, *J. Quant. Spectrosc. Radiat. Transfer*, *70*, 761–776, doi:10.1016/S0022-4073(01)00044-9.

Muinonen, K. (1989), Scattering of light by crystals: A modified Kirchhoff approximation, *Appl. Opt.*, *28*, 3044–3050, doi:10.1364/AO.28.003044.

Ono, A. (1969), The shape and riming properties of ice crystals in natural clouds, *J. Atmos. Sci.*, *26*, 138–147, doi:10.1175/1520-0469(1969)026<0138:TSARPO>2.0.CO;2.

Pruppacher, H. P., and J. D. Klett (1980), *Microphysics of Clouds and Precipitation*, 714 pp., D. Reidel, Norwell, Mass.

Purcell, E. M., and C. R. Pennypacker (1973), Scattering and absorption of light by nonspherical dielectric grains, *Astrophys. J.*, *186*, 705–714, doi:10.1086/152538.

Reagan, J. A., X. Wang, and M. T. Osborn (2002), Spaceborne lidar calibration from cirrus and molecular backscatter returns, *IEEE Trans. Geosci. Remote Sens.*, *40*, 2285–2290, doi:10.1109/TGRS.2002.802464.

Takano, Y., and K. N. Liou (1989), Solar radiative transfer in cirrus clouds. Part I: Single-scattering and optical properties of hexagonal ice crystals, *J. Atmos. Sci.*, *46*, 3–19, doi:10.1175/1520-0469(1989)046<0003:SRTICC>2.0.CO;2.

Tao, Z. M., M. P. McCormick, D. Wu, Z. Y. Liu, and M. A. Vaughan (2008), Measurements of cirrus cloud backscatter color ratio with a two-wavelength lidar, *Appl. Opt.*, *47*, 1478–1485, doi:10.1364/AO.47.001478.

van de Hulst, H. C. (1957), *Light Scattering by Small Particles*, John Wiley, Hoboken, N. J.

Vaughan, M. A., M. J. McGill, Z. Liu, Y. Hu, R. E. Kuehn, and S. D. Rodier (2008), Backscatter color ratios of cirrus clouds measured by the cloud physics lidar, paper presented at 15th International Conference on Clouds and Precipitation, Int. Comm. on Clouds and Precip., Mexico City. (Available at http://cabernet.atmosfcu.unam.mx/ICCP-2008/abstracts/Program_on_line/Poster_13/Vaughan_extended.pdf)

Warren, S. G., and R. E. Brandt (2008), Optical constants of ice from the ultraviolet to the microwave: A revised compilation, *J. Geophys. Res.*, *113*, D14220, doi:10.1029/2007JD009744.

Winker, D. M., J. R. Pelon, and M. P. McCormick (2003), The CALIPSO mission: Spaceborne lidar for observation of aerosols and clouds, *Proc. SPIE Int. Soc. Opt. Eng.*, *4893*, 1–11, doi:10.1117/12.466539.

Yang, P., and K. N. Liou (1996a), Finite-difference time domain method for light scattering by small ice crystals in three-dimensional space, *J. Opt. Soc. Am. A Opt. Image Sci. Vis.*, *13*, 2072–2085, doi:10.1364/JOSAA.13.002072.

Yang, P., and K. N. Liou (1996b), Geometric-optics–integral-equation method for light scattering by nonspherical ice crystals, *Appl. Opt.*, *35*, 6568–6584, doi:10.1364/AO.35.006568.

Yang, P., B. C. Gao, B. A. Baum, Y. X. Hu, W. J. Wiscombe, S. C. Tsay, D. M. Winker, and S. L. Nasiri (2001), Radiative properties of cirrus clouds in the infrared (8–13 μm) spectral region, *J. Quant. Spectrosc. Radiat. Transfer*, *70*, 473–504, doi:10.1016/S0022-4073(01)00024-3.

Yang, P., H. L. Wei, H. L. Huang, B. A. Baum, Y. Hu, G. W. Kattawar, M. I. Mishchenko, and Q. Fu (2005), Scattering and absorption property database for nonspherical ice particles in the near- through far-infrared spectral region, *Appl. Opt.*, *44*, 5512–5523, doi:10.1364/AO.44.005512.

Yang, P., Q. Feng, G. Hong, G. W. Kattawar, W. J. Wiscombe, M. I. Mishchenko, O. Dubovik, I. Laszlo, and I. N. Sokolik (2007), Modeling of the scattering and radiative properties of nonspherical dust particles, *J. Aerosol Sci.*, *38*, 995–1014, doi:10.1016/j.jaerosci.2007.07.001.

Yee, K. S. (1966), Numerical solution of initial boundary value problems involving Maxwell's equations in isotropic media, *IEEE Trans. Antennas Propag.*, *14*, 302–307, doi:10.1109/TAP.1966.1138693.

B. A. Baum, Space Science and Engineering Center, University of Wisconsin-Madison, Madison, WI 53706, USA.

L. Bi and G. W. Kattawar, Department of Physics, Texas A&M University, College Station, TX 77843, USA.

R. S. Brock and J. Q. Lu, Department of Physics, East Carolina University, Greenville, NC 27858, USA.

Y. X. Hu and D. M. Winker, NASA Langley Research Center, Hampton, VA 23681, USA.

P. Yang, Department of Atmospheric Sciences, Texas A&M University, 3150 TAMU, College Station, TX 77843, USA. (pyang@ariel.met.tamu.edu)